


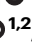
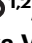

# Vasculogenic skin reprogramming requires TET-mediated gene demethylation in fibroblasts for rescuing impaired perfusion in diabetes

Received: 12 May 2024

Accepted: 7 November 2024

Published online: 27 November 2024

 Check for updates

Sujit K. Mohanty<sup>1,2,3,6</sup>, Kanhaiya Singh<sup>1,2,3,6</sup>, Manishekhar Kumar<sup>1,2,3</sup>, Sumit S. Verma<sup>1,2,3</sup>, Rajneesh Srivastava<sup>1,2,3</sup>, Surya C. Gnyawali <sup>1,2,3</sup>, Ravichand Palakurti<sup>1,2,3</sup>, Ajay K. Sahi<sup>1,2</sup>, Mohamed S. El Masry <sup>1,2</sup>, Pradipta Banerjee<sup>1,2</sup>, Sedat Kacar <sup>3</sup>, Yashika Rustagi<sup>3</sup>, Priyanka Verma<sup>3</sup>, Subhadip Ghatak<sup>1,2,3</sup>, Edward Hernandez<sup>3</sup>, J. Peter Rubin<sup>1,4,5</sup>, Savita Khanna<sup>1,2,3</sup>, Sashwati Roy<sup>1,2,3</sup>, Mervin C. Yoder<sup>1,2,3</sup> & Chandan K. Sen <sup>1,2,3,4</sup> ✉

Tissue nanotransfection (TNT) topically delivers *Etv2*, *Foxc2*, and *Fli1* (EFF) plasmids increasing vasculogenic fibroblasts (VF) and promoting vascularization in ischemic murine skin. Human dermal fibroblasts respond to EFF nanoelectroporation with elevated expression of endothelial genes in vitro, which is linked to increased ten-eleven translocase 1/2/3 (TET) expression. Single cell RNA sequencing dependent validation of VF induction reveals a TET-dependent transcript signature. TNT<sub>EFF</sub> also induces TET expression in vivo, and fibroblast-specific EFF overexpression leads to VF-transition, with TET-activation correlating with higher 5-hydroxymethylcytosine (5-hmC) levels in VF. VF emergence requires TET-dependent demethylation of endothelial genes in vivo, enhancing VF abundance and restoring perfusion in diabetic ischemic limbs. TNT<sub>EFF</sub> improves perfusion and wound closure in diabetic mice, while increasing VF in cultured human skin explants. Suppressed in diabetes, TET1/2/3 play a critical role in TNT-mediated VF formation which supports de novo blood vessel development to rescue diabetic ischemic tissue.

The generation of cells of desired functionality to replace or repair aging, diseased, or damaged tissues is of outstanding interest<sup>1,2</sup>. Direct lineage reprogramming, i.e., direct induction of functional cell types from one lineage to phenotype and function of another lineage, circumvents intermediary pluripotent state reprogramming and related risks<sup>1,3</sup>, and represents an attractive approach to repair and rescue

tissue functionality<sup>4</sup>. Direct cell reprogramming relies on the use of lineage-specific transcription factors (TF) to recreate the conditions necessary for converting cells from one cell lineage to another. Thus, choice of TF for direct reprogramming are generally identified through the study of cell lineage specification during development<sup>5</sup>. Capitalizing on these developmental cues, previously reported works have

<sup>1</sup>McGowan Institute for Regenerative Medicine, University of Pittsburgh, Pittsburgh, PA, USA. <sup>2</sup>Department of Surgery, University of Pittsburgh, Pittsburgh, PA, USA. <sup>3</sup>Indiana Center for Regenerative Medicine and Engineering, Indiana University School of Medicine, Indianapolis, IN, USA. <sup>4</sup>Department of Plastic Surgery, University of Pittsburgh, Pittsburgh, PA, USA. <sup>5</sup>Department of Bioengineering, University of Pittsburgh, Pittsburgh, PA, USA. <sup>6</sup>These authors contributed equally: Sujit K. Mohanty, Kanhaiya Singh. ✉ e-mail: [c.k.sen@pitt.edu](mailto:c.k.sen@pitt.edu)

utilized ETV2, ERG, FLI1, DKK3 and TAL1 to directly generate endothelial-like cells from a variety of different somatic cell host lineages<sup>6–9</sup>.

Fibroblasts are ubiquitous and were thought to display lower epigenetic barriers and thus are well suited for conversion into a variety of functionally targeted cell states<sup>5,10</sup>. ETS transcription factors are potent regulators of vascular development and angiogenesis<sup>11</sup>. Direct reprogramming of fibroblasts to generate endothelial-like cells using ETS family of TF (e.g., *Etv2*, *Fli1*) has been reported<sup>12</sup>. Earlier studies have employed the *ETV2/FLI1/ERG1* cocktail to achieve generation of endothelial-like cells from fibroblasts in vitro<sup>8,13</sup>. Several other in vitro studies have used various combinations of *Etv2* and *Fli1* either alone or together with factors such as *Foxo1*, *Klf2*, *Tal1*, and *Lmo2* to generate endothelial-like cells<sup>7,13</sup>. These endothelial-like cells were transplanted into mouse ischemic hindlimbs to induce new vessel formation. Vascular tissue engineering approaches based on endothelial cell conversion in vitro face the challenge of transplantation, graft acceptance and inosculation<sup>14</sup>. Work reported from our laboratories, have demonstrated that TNT-based vasculogenic reprogramming of the skin in vivo requires a hypoxic microenvironment in the tissue<sup>15,16</sup>. This approach obviates the need for transplantation and elaborate laboratory infrastructure for in vitro processing of cell-based therapies. Furthermore, in vivo reprogramming occurs in the living body under immune surveillance resulting in sustainable inducible vasculogenesis without host immunologic elimination<sup>5,16</sup>. To that end, we are committed to developing viable alternative approaches as options for translational development. Our previous works have identified that tissue nanotransfection (TNT) based topical electrophoretic delivery of *Etv2*, *Foxc2*, and *Fli1* (EFF cocktail)<sup>16,17</sup> plasmids achieve induced vascular perfusion in the skin. When first reported<sup>16</sup>, we interpreted TNT<sub>EFF</sub> outcome as a fate-change of fibroblasts to endothelial-like cells in vivo. Based on more recent single cell RNA sequencing (scRNA-seq) studies we now know that instead it is a state-change of dermal fibroblasts to vasculogenic fibroblasts (VF) in vivo, which in turn participate as components of functional blood vessels<sup>15</sup>. VF is an injury-inducible, TNT-responsive, adaptive physiological state change aimed at tissue repair<sup>15</sup>. Elucidation of the underlying cellular and molecular mechanisms producing VF in response to TNT<sub>EFF</sub> will help maximize the benefits of rescuing perfusion to ischemic skin and in achieving translational success.

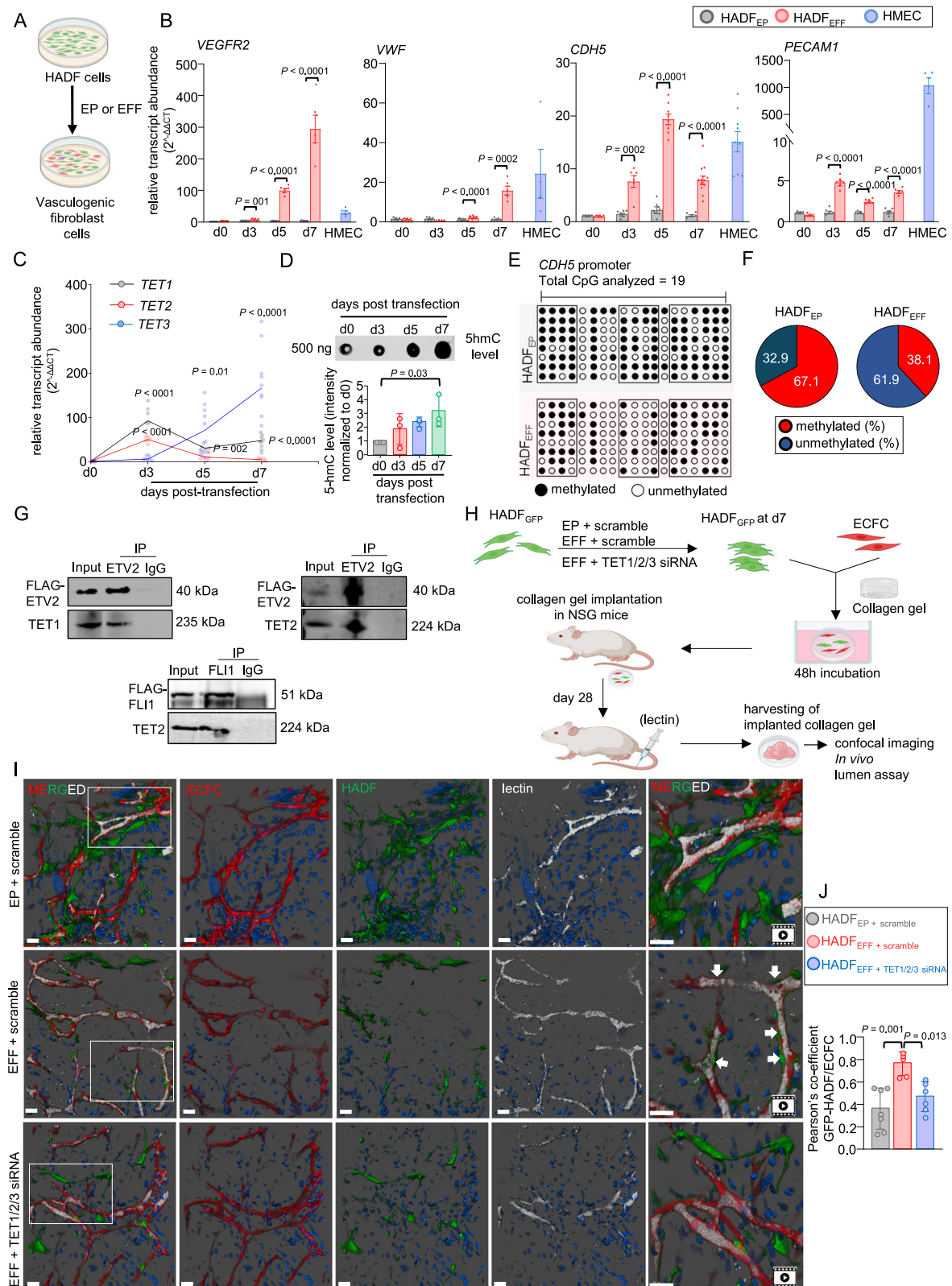
During reprogramming, TF plays essential roles in the binding of epigenetic regulators and recruitment of the regulatory complex to specific regions on the genomic DNA<sup>18</sup> to promote demethylation of responsive genes, and collectively activate gene expression to modify the cell state<sup>19</sup>. TF interact with epigenetic regulators during vascular development or regeneration<sup>20</sup>. However, it is still unclear whether this interplay between DNA methylation and TF binding is restricted to enhancing endothelial gene transcription or does it play a wider role in decisions towards cell-state conversion. DNA methyltransferases (DNMTs), in combination with chromatin state, regulate DNA methylation to repress or maintain gene expression<sup>21</sup>. DNA demethylation induces transcription and is regulated by ten-eleven translocation 1-3 (TET1/2/3) methylcytosine dioxygenases, which oxidize 5-methylcytosine to unmodified cytosine either by active or passive demethylation mechanisms<sup>19</sup>. During TF-induced fibroblast to endothelial-like cell change, hypomethylation of the proximal promoters of several endothelial-specific genes has been observed<sup>6,7</sup>. However, the significance of TET1/2/3 in mediating selective demethylation of the typically “vascular” genes in fibroblasts is poorly understood. Furthermore, the potential role of TET1/2/3 in the epigenetic dysregulation, that is observed in diabetes, causing hypermethylation of endothelial genes and vascular dysfunction remains to be delineated<sup>22</sup>. Our previous work supports the notion that EFF functions as a vasculogenic agent in adult skin inducing the formation of functional blood vessels<sup>16</sup>.

In the current work, we tested the hypothesis that active demethylation of fibroblast-borne endothelial genes is a prerequisite for EFF-induced vasculogenesis. This work provides the evidence that TET1/2/3 expression in dermal fibroblasts reduces promoter-methylation of fibroblast-borne endothelial genes thus resulting in the emergence of a novel VF subset. Augmenting VF abundance, naturally deficient in diabetic ischemic tissue, improves perfusion of the injured tissue thus rescuing poorly healing diabetic cutaneous wounds.

## Results

### The vasculogenic state of human adult dermal fibroblast is TET-dependent

As physiological response to injury or wounding, we observed the upregulation of endogenous EFF in day 5 WE tissue (Fig. S1A–C). Specifically, COL1A2<sup>+</sup> dermal fibroblasts of WE showed increased expression of EFF (Fig. S1D, E). In vitro studies on human adult dermal fibroblasts (HADF) were conducted to understand the significance of EFF overexpression. EFF open reading frames (ORF<sub>EFF</sub>) were delivered to HADF leading to significant increases in each TF compared to empty plasmid control treatment (Fig. S2A, B). Comparison of the delivery of each individual TF, pairs of TF, or a combined EFF treatment revealed that the EFF cocktail caused the most significant induction of vasculogenic genes (*VEGFR2*, *PECAMI* and *CDH5*) in normoglycemic and hyperglycemic (50 mM D-glucose) culture conditions (Fig. 1A, B; Fig. S2C–F). Of interest, the hyperglycemic conditions blunted the magnitude of the EFF effect on transcript abundance compared to the osmolarity control samples (Fig. S2E, F). Interestingly, these EFF-transfected HADF retained fibroblast features as explained by the high abundance of *COL1A2*, an abundant fibroblast product and marker on days 5 and 7 post-transfection (Fig. S3A, B). Hence, these cells are called vasculogenic fibroblasts (VF<sub>EFF</sub>) consistent with our previous report. To test whether TNT<sub>EFF</sub> is capable of inducing VF in the human skin, we studied ex vivo cultured human skin explants. Surgically discarded and de-identified human skin samples were obtained from individuals undergoing surgery and processed for human skin ex vivo culture. We obtained data from human skin ex vivo cultures treated with TNT<sub>EP</sub> ( $n = 9$  grafts from 5 individuals) or TNT<sub>EFF</sub> ( $n = 10$  grafts from the same 5 individuals). The blood vessel density (Fig. S3C) and COL1A2/VWF colocalization (Fig. S3D) was significantly higher on day 7 in TNT<sub>EFF</sub> treated skin ex vivo grafts as compared to TNT<sub>EP</sub> treated grafts. These initial studies demonstrate TNT<sub>EFF</sub> delivery in ischemic human skin explants significantly increases VF, and these results are consistent with EFF-induced VF derived from isolated dermal fibroblast cultures. Next, we sought to understand the mechanistic underpinnings of such fibroblast→VF transition and our attention was drawn towards plausible epigenetic alterations orchestrated by EFF overexpression. ETV2-TET1/2 dependent DNA demethylation has been reported to increase endothelial-specific gene expression in non-endothelial cells. In the present study, VF<sub>EFF</sub> emergence was associated with increased transcript abundance of *TET1/2/3* (Fig. 1C). However, the transcript abundance of *DNMTs* were not significantly different compared to EP control treated HADF (Fig. S3C) leading us to focus on EFF and TET1/2/3 interactions in mediating VF<sub>EFF</sub> induction. Abundance of *TET1/2/3* in WE tissue were also found to significantly increase during physiological wound healing processes specifically in the COL1A2 rich dermal fibroblast compartment (Fig. S4A–D). Such increased transcript abundance of *TET1/2/3* was associated with higher levels of 5-hydroxymethylcytosine (5-hmC) abundance in VF<sub>EFF</sub> (Fig. 1D). Additionally, significantly lower methylation in the promoter of the endothelial-specific *CDH5* gene was observed in VF<sub>EFF</sub> (38.1%) as compared to HADF<sub>EP</sub> (67.1%) (Fig. 1E, F). To identify the mechanism of epigenetic regulation post-EFF induction of VF<sub>EFF</sub>, direct interaction of EFF-TET protein were



analyzed using a Flag-based co-immunoprecipitation (co-IP) strategy. ETV2 directly interacted with both TET1 and TET2. However, FLI1 interacted with only TET2 in V<sub>EFF</sub> post-72h of EFF transfection (Fig. 1G). FOXC2 did not directly interact with either of these TET (Fig. S5A). These results support that TET1 and/or 2 proteins directly interact with ETV2 and FLI1 (EF) and are associated with vasculogenic

gene demethylation and subsequent increased endothelial transcript abundance in V<sub>EFF</sub> cells. To investigate the causal relationship of TET1/2/3 in V<sub>EFF</sub> conversion, siRNA mediated TET1/2/3 knockdown in EFF-treated HADF was tested (Fig. S5B, C). TET1/2/3 knockdown during concomitant EFF overexpression, blunted V<sub>EFF</sub> emergence by repressing vasculogenic genes (*VEGFR2*, *PECAM1*, and *CDH5*) in



**Fig. 1 | The vasculogenic state of human adult dermal fibroblast is TET-dependent.** **A** Schematic diagram of *ETV2*, *FLII* and *FOXC2* (*EFF*) plasmids delivery in HADF (*HADF<sub>EFF</sub>*) and empty plasmid (*EP*) control. Positive control = HMEC cells. **B** *VEGFR2* (*d0* (*n* = 6, 6); *d3* (*n* = 6, 6); *d5* (*n* = 5, 5); *d7* (*n* = 6, 5); *HMEC*, *n* = 4)], *VWF* (*d0*, *n* = 6, 6; *d3*, *n* = 6, 4; *d5*, *n* = 8, 10; *d7*, *n* = 5, 5; *HMEC*, *n* = 4), *CDH5* (*d0*, *n* = 6, 6; *d3*, *n* = 6, 6; *d5*, *n* = 6, 8; *d7*, *n* = 5, 12; *HMEC*, *n* = 9), and *PECAM1* (*d0*, *n* = 6, 6; *d3*, *n* = 5, 6; *d5*, *n* = 5, 5; *d7*, *n* = 5, 5; *HMEC*, *n* = 4) transcript abundance in *HADF<sub>EFF</sub>* and *HADF<sub>EP</sub>* treated cells at days 0, 3, 5, and 7 post-transfection. Results represent mean  $\pm$  S.D (Student *t* test, two-sided). **C** *TET1*, *TET2*, and *TET3* transcript abundance in *EFF* treated HADF cells at days 0 (*n* = 5, 6, 7), 3 (*n* = 6, 6, 6), 5 (*n* = 6, 6, 10) and 7 (*n* = 8, 7, 10) post-transfection. Results represent mean  $\pm$  S.D. One-way ANOVA, Tukey HSD post-hoc-test (**D**) Dot blot (top) and its intensity analysis (below) of 5-hydroxymethylcytosine (5-hmC) analyzed in *EFF* treated HADF cells at days 0, 3, 5, and 7 post-transfection. Results represent mean  $\pm$  S.D (*n* = 3; Student *t* test, two-sided). **E** *CDH5* promoter methylation status in *HADF<sub>EP</sub>* and *HADF<sub>EFF</sub>* treated HADF cells at d7. Clones analyzed = 6. **F** Venn diagram shows *CDH5* methylation in *HADF<sub>EP</sub>* (Left) and *HADF<sub>EFF</sub>*

(Right) at d7. **G** Co-immunoprecipitation experiments performed with anti-*ETV2* and anti-*TET1* (left) and *TET2* (right) antibodies on HADF cells treated with Flag-*ETV2*. A different set of interaction was assessed using Flag-*FLII* transfected in HADF cells using antibodies against *FLII* and *TET2*. **H** Experimental design for in vivo collagen gel assay. **I, J** Immunofluorescence confocal images and analysis of in vivo collagen gel assay showing more prevalence of lectin (white) perfused vessels of HADF (green) origin treated with *EFF*+scramble siRNA at day 28 as compared to *EP*+scramble. ECFC cells are shown in red. **I** Such perfused vessels were absent in *EFF*+*TET1/2/3* siRNA group where HADF cells were treated with *TET1/2/3* siRNA in presence of *EFF*. Scale, 50  $\mu$ m. **J** The rightmost panel represents the colocalization of HADF-GFP, lectin, and ECFC-tdTomato in the 3D cross-sectional view rendered by IMARIS. Results represent mean  $\pm$  S.D. (*n* = 7, 5, 6; one-way ANOVA, Tukey HSD post-hoc-test). Source data are provided as a Source Data file. *n* = biological replicates in (**B**, **C**, **D**, **J**). **A**, **H** are created in BioRender. Mohanty, S. (2024) BioRender.com/024n391. indicates Supplementary Movie 1–3.

*EFF*-treated HADFs (Fig. S5D). Failure to observe *EFF*-induced increase in HADF *CDH5* transcripts was consistent with no change in *CDH5* promoter DNA methylation in *TET1/2/3* siRNA treated HADF cells in response to *EFF* overexpression (*EP*+scramble = 69.5%; *EFF*+scramble = 34.2%; *EP*+*TET1/2/3* siRNA = 72.8%; and *EFF*+*TET1/2/3* siRNA = 71%) (Fig. S5E). Thus, *TET1/2/3* are required for *EFF*-dependent VF induction in vitro.

To investigate the functional significance of *TET1/2/3*-dependent induction of vasculogenic characteristics in *VF<sub>EFF</sub>*, commercially available HADF expressing green fluorescent protein (GFP) were transfected with *EFF* ORF in the presence or absence of TET. These cells were then suspended along with tdTomato<sup>+</sup> cord blood endothelial colony forming cells (ECFC) (1:1 ratio with ECFC as positive control) in collagen gels, cultured in vitro for 48 h, and then implanted within the subcutaneous space of immunodeficient mice. After 28 days, confirmation of intravenously delivered lectin-perfused chimeric capillary vessels comprised of human vasculogenic fibroblast (*VF<sub>EFF</sub>*) and some tdTomato<sup>+</sup> ECFC cells was detected in 5 of 7 test mice (Fig. 1H–J). This perfused chimeric capillary formation ability of *VF<sub>EFF</sub>* was lost when *TET1/2/3* transcripts were knocked down during this experimental setting (Fig. 1H–J). Thus, some HADF attained vasculogenic capacity as *VF<sub>EFF</sub>* and yet retained fibroblast cell transcripts in response to exogenous *EFF* delivery (Fig. S3A, B). Here, *VF<sub>EFF</sub>* vasculogenic function is suggestive of a fibroblast subset state change in a TET-dependent fashion.

### Single-cell RNA sequencing (scRNA-seq) analysis reveal TET-dependent gain of a vasculogenic cluster in dermal fibroblasts in response to *EFF* delivery

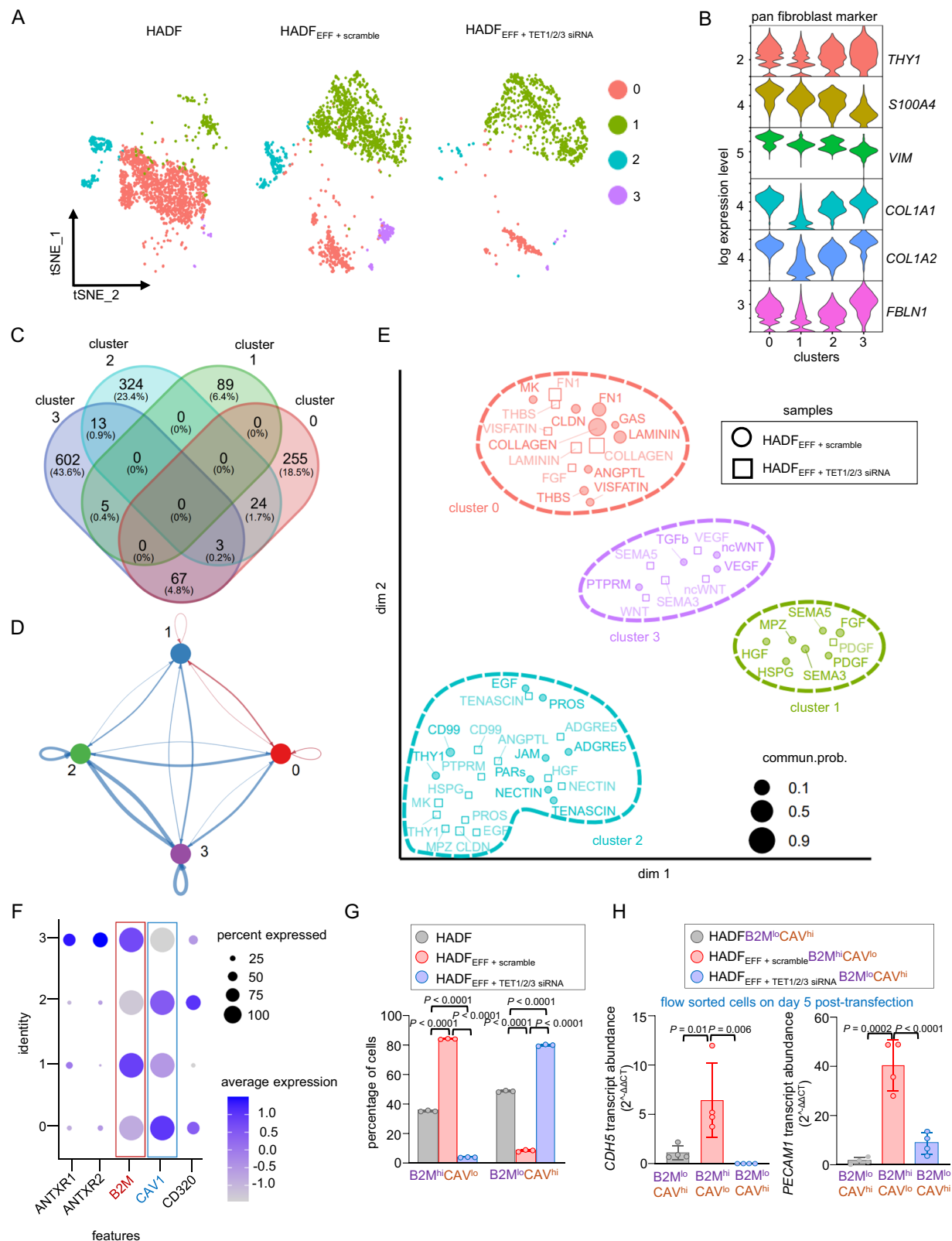
In in vitro studies, to interrogate single-cell HADF transcriptome complexity, all cells from *EFF*-transfected d5 HADF were compared in the presence and absence of *TET1/2/3*-siRNAs. Parental HADF cells with no treatment were used as additional baseline controls for scRNA-seq analysis. The initial dataset contained 18624 cells including 7978 cells that met quality control parameters and underwent downstream analysis. Unsupervised clustering identified 4 clusters (Fig. 2A). Compositional analysis revealed that clusters 1 and 3 cells increased in response to *EFF* transfection. Cluster 3 was identified as a TET-dependent cluster, as this cluster was lost after *TET1/2/3* siRNA-treatment (Fig. 2A). All four clusters identified above displayed pan-fibroblast markers *THY1*, *SIOO44*, *VIM*, *COLIA2*, *COL1A1* and *FBLN1* (Fig. 2B). The interaction of differentially expressed genes (DEG) identified in individual clusters compared to others is illustrated (Fig. 2C). Cluster 3 was the most unique cluster containing ~44% of total DEG among the compared groups. Differential connectome analysis using CellChat was performed between clusters post-*EFF* transfection in the presence or absence of *TET1/2/3* siRNA. Overall cell-cell communication between HADF clusters was diminished in *EFF*-transfected

HADF post-*TET1/2/3* inhibition (Fig. 2D, Fig. S6A, B). Degree of functional similarity of the contributing signaling pathways or ligand-receptor pairs identified was determined using the joint manifold learning and classification of the inferred communication networks (Fig. 2E). A significant enrichment of transcripts involved in VEGF, PDGF, and SEMA pathways was detected in clusters 1 and 3 (Fig. 2E). Such enrichment was lost in cluster 3 in response to *TET1/2/3* inhibition. Analysis of cell surface proteins in all four clusters identified cluster 1 and 3 as beta 2 microglobulin high (*B2M<sup>hi</sup>*) and Caveolin 1 low (*CAV<sup>lo</sup>*) while the remaining clusters were *B2M<sup>lo</sup>* *CAV<sup>hi</sup>* (Fig. 2F, Fig. S6C). Flow-sorting followed by expression analysis of these identified vasculogenic clusters (cluster 1 and 3; *B2M<sup>hi</sup>* *CAV<sup>lo</sup>*) exhibited high abundance of endothelial transcripts (*CDH5* and *PECAM1*); both of which were lost in response to *TET1/2/3* inhibition (Fig. 2G, H, Fig. S6D). Thus, under in vitro conditions, a *TET1/2/3*-dependent fibroblast subcluster displaying vasculogenic transcripts emerges from HADF treated with *EFF*.

### TET-dependent induction of vasculogenic state of fibroblasts require demethylation of fibroblast-borne endothelial genes in vivo

We first examined the functional significance of exogenous *EFF* and TET induction by experimental induction of ischemia in the hind limb (HLI) of C57BL/6 mice (Fig. 3A). Topical TNT-based *EFF* delivery (*TNT<sub>EFF</sub>*) rescued HLI with significantly improved perfusion as measured by high resolution laser speckle imaging (LSI) (Fig. 3B, C) and ultrasound imaging (Fig. 3D, E) compared to *TNT<sub>EP</sub>* control delivery. We have previously established that due to *TNT<sub>EFF</sub>*, angiogenesis was also induced in more distal locations within the limb, such as the gastrocnemius muscle<sup>16</sup>. Enhanced perfusion of the ischemic limb post-*EFF* transfection was significantly abrogated when *TET1/2/3* were silenced (Fig. 3B–E). In addition, the histological abundance of increased *COLIA2<sup>+</sup>* *VWF<sup>+</sup>* *VF<sub>EFF</sub>* in response to *EFF* transfection was also reduced to basal levels when *TET1/2/3* were silenced in HLI (Fig. 3F). Bisulfite sequencing of the DNA isolated from dermal fibroblasts (*COLIA2<sup>+</sup>*) of the ischemic skin revealed that promoter regions of vasculogenic genes *Cdh5* (32.6% vs 67.4%), *Vwf* (23.7% vs 76.3%) and *Pecam1* (42.8% vs 57.2%) were hypomethylated in response to *EFF* transfection as compared to *EP* controls, respectively (Fig. 3G). *EFF* effects on vascular gene demethylation in ischemic tissue was lost when *TET1/2/3* were inhibited (*Cdh5*, 69.8%; *Vwf*, 86.8%; *Pecam1*, 75.5%) (Fig. 3G). Thus, optimal *TET1/2/3* abundance in dermal *COLIA2<sup>+</sup>* elements transfected with topical *TNT<sub>EFF</sub>* delivery resulted in substantial in vivo induction of fibroblast  $\rightarrow$  *VF<sub>EFF</sub>* state that improved tissue perfusion.

In recognition of the possibility that deeper skeletal muscle fibroblasts or adventitial femoral artery fibroblasts may have contributed to the above-mentioned improvement in perfusion, we turned towards a full-thickness cutaneous injury model to examine the



role of *EFF* treatment and its impact on skin perfusion and wound closure (Fig. S7A, B). In response to TNT<sub>EFF</sub>, *EFF*, and *Pecam1* transcript abundance was increased in skin COL1A2<sup>+</sup> tissue elements but no change was observed in keratinocytes (K14<sup>+</sup>) and endothelial (CDH5<sup>+</sup>) cells of TNT<sub>EFF</sub> treated skin (Fig. S7C, D). TNT<sub>EFF</sub> also increased the abundance of active TET1/2/3 at the WE, and resulted in increased perfusion and accelerated wound closure (Figs S7E, F and S8A–E). The

beneficial effect of *EFF* on wound perfusion and healing was abrogated when *TET1/2/3* were inhibited under the same experimental conditions (Fig. S8A–E). In addition, the transcript abundance of vasculogenic genes (Fig. S8F) and histological abundance of increased COL1A2<sup>+</sup>/VWF<sup>+</sup> V<sub>EFF</sub> in response to *EFF* transfection were also reduced to basal levels when *TET1/2/3* were silenced at the d14 WE (Fig. S8G). These observations establish that the vasculogenic state change is

**Fig. 2 | Single-cell RNA sequencing analysis reveals TET-dependent gain of a vasculogenic cluster in dermal fibroblasts in response to *Etv2*, *Foxc2* and *Fli1* transfection.** **A** t-SNE plots for HADF cells at day 5 post EFF transfection in the presence or absence of TET1/2/3 siRNA. Parent HADF cells were used as d0 control. Unsupervised clustering identified 4 cell clusters (0, 1, 2, 3). The abundance of clusters 1 ( $P < 0.00001$ ) and 3 ( $P < 0.00001$ ) increased at d5 post-EFF transfection. Chi-Square test, two sided. Cluster 3 was identified as TET1/3 dependent cluster which was lost after treatment with TET1/2/3 siRNA.  $P < 0.00001$ , Chi-Square test, two sided. **B** Violin plots expression of pan-fibroblast markers representing clusters 1 and 3 retained their fibroblast gene signature **(C)** Intersection of DEG ( $\log_2FC \geq 0.58$ , adj.  $p \leq 0.01$ , Wilcoxon Rank Sum Test, two-sided) identified in individual clusters compared to others were illustrated in Venn diagram. **D** Differential connectome analysis using CellChat between fibroblast clusters post-EFF transfection in the presence or absence of TET1/2/3 siRNA. Diagram showing communication network where the blue indicates less while red indicates more signals between fibroblast clusters

post-TET1/2/3 siRNA inhibition. Overall cell-cell communication between HADF clusters were diminished in EFF transfected HADFs post-TET1/2/3 siRNA inhibition as marked by the presence of more blue lines. **E** Degree of functional similarity of the contributing signaling pathways (weighted senders and receivers) or ligand-receptor pairs identified between fibroblast clusters post-EFF transfection in the presence or absence of TET1/2/3 siRNA. Due to the enrichment of VEGF, PDGF, and SEMA pathways Clusters 1 and 3 were identified as vasculogenic cluster out of which cluster 3 was TET1/2/3 siRNA dependent. **F** Dot plot representing different membrane receptors specific to identified clusters in **(A)**. **G** Flow sorting of vasculogenic clusters (1 and 3; B2M<sup>hi</sup>CAV<sup>lo</sup>) and rest of other clusters (0 and 2; B2M<sup>lo</sup>CAV<sup>hi</sup>). Results represent mean  $\pm$  SD. ( $n = 3$ ).  $P < 0.05$  (oneway ANOVA, Tukey HSD post hoc test) **(H)** *CDH5* and *PECAM1* transcript abundance in B2M<sup>hi</sup>CAV<sup>lo</sup> and B2M<sup>lo</sup>CAV<sup>hi</sup> sorted cells. Results represent mean  $\pm$  SD. ( $n = 4$ ).  $n =$  biological replicates in **(G, H)**. Oneway ANOVA, Tukey HSD post hoc test. Source data are provided as a Source Data file.

dependent upon TET1/2/3 expression. The long-term effect of TNT<sub>EFF</sub> was tested by analyzing the full-thickness cutaneous wound till day 28 post-wounding. While some physiologic emergence of COL1A2<sup>+</sup> cells that co-localized with lectin perfused vessels was apparent with significant increase in perfusion (Fig. S8H–M), as might be expected, the increase in endothelial transcripts (*Vwif*, *Pecam1*) as seen at day 14 (Fig. S8F) was not observed in the fibroblast elements captured from the wound-edge (Fig. S8M). However, corresponding endothelial protein (*Vwif*) persisted in such lectin colocalized COL1A2<sup>+</sup> cells (Fig. S8N). Thus, the TNT<sub>EFF</sub> mediated effect on increasing blood flow persists while the endothelial transcripts are diminishing by day 28.

### Fibroblast-specific inducible overexpression of EFF causes induction of TET, which is followed by transition to vasculogenic fibroblast in vivo

Seeking direct evidence of VF<sub>EFF</sub> cell state conversion in vivo, HLI studies were conducted in a TARGATT inducible EFF<sup>fl/fl</sup>Col1a2<sup>CreER</sup> mouse strain in both sexes (Fig. S9A–C). To produce this mouse line, the mammalian *Etv2*, *Foxc2*, and *Fli1* open reading frames were inserted into an established TARGATT vector (Applied StemCell, Milpitas, CA). These ORFs were placed under the control of floxed SV40 stop codon to require inducible expression. The *Col1a2*<sup>CreER</sup> transgenic driver mouse was chosen since COL1A2 is widely expressed among dermal fibroblasts (Fig. 2B). In cutaneous wound studies, application of tamoxifen to WE tissue in EFF<sup>fl/fl</sup>Col1a2<sup>CreER</sup> mice deleted the LoxP flanked stop cassette in the TARGATT mouse and induced EFF and TET1/2/3 expression at the affected skin-site (Fig. S9D–H). Such treatment improved blood-flow, accelerated wound closure and increased COL1A2<sup>+</sup>VF<sub>EFF</sub><sup>+</sup> VF<sub>EFF</sub> abundance (Fig. S9I–M). Tamoxifen treatment in the HLI of EFF<sup>fl/fl</sup>Col1a2<sup>CreER</sup> TARGATT mouse improved perfusion and blood flow to the ischemic limb (Fig. 4A–D). In this TARGATT experimental system, the effect of tamoxifen as an active principle was assessed using additional EFF<sup>fl/fl</sup> control mice. No significant change in wound perfusion, closure and COL1A2<sup>+</sup>VF<sub>EFF</sub><sup>+</sup> VF<sub>EFF</sub> abundance was noted in tamoxifen treated EFF<sup>fl/fl</sup> control mice (Fig. S9I–M). Tamoxifen treated EFF<sup>fl/fl</sup>Col1a2<sup>CreER</sup> and EFF<sup>fl/fl</sup> mice were thus selected as experimental groups for further studies.

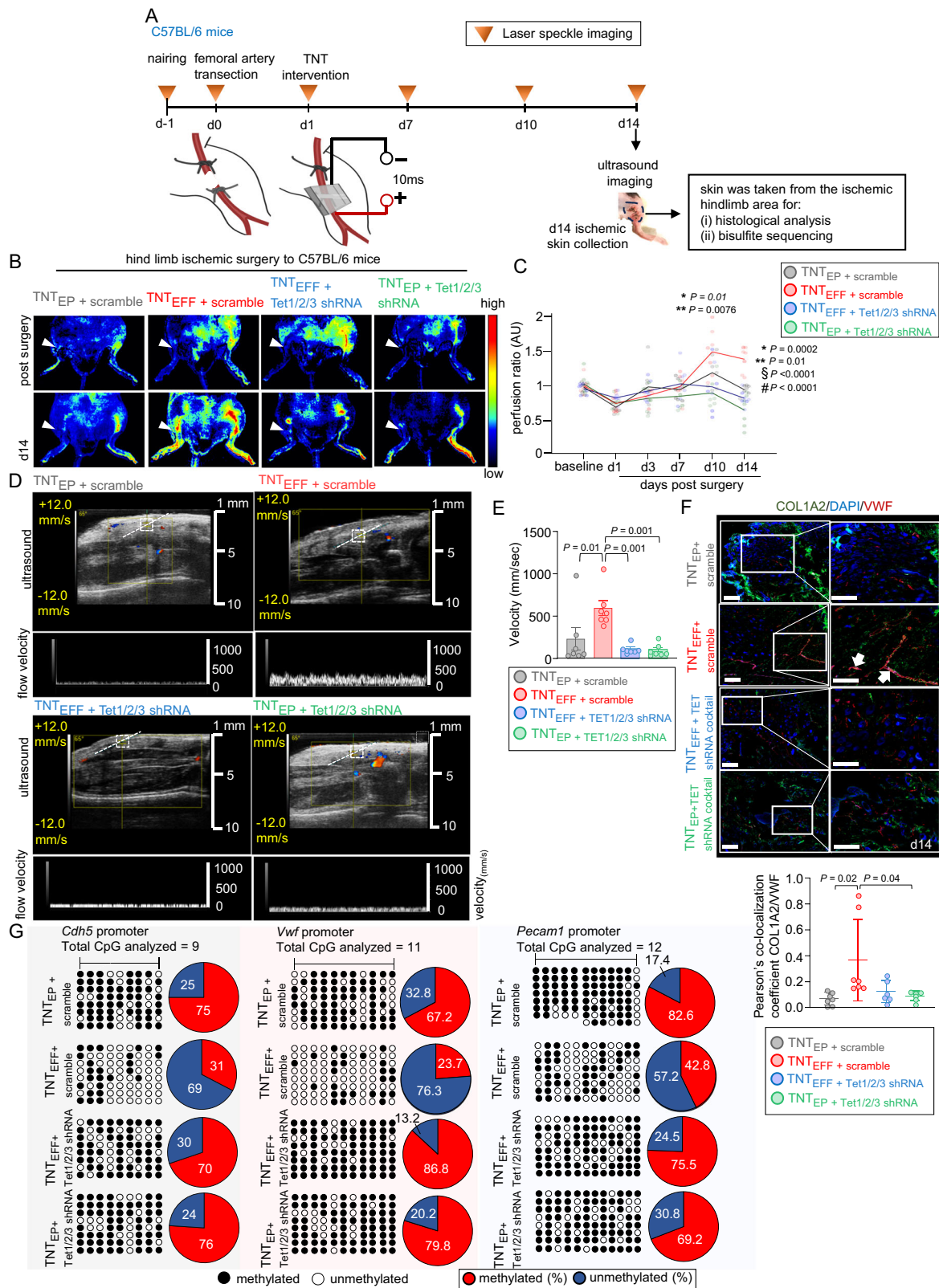
To evaluate the genetic involvement of TET1/2/3 in EFF-induced VF formation from fibroblasts, *Tet1*, *Tet2*, and *Tet3* triple-floxed mice were crossed with EFF<sup>fl/fl</sup>Col1a2<sup>CreER</sup> mice (hereafter referred to as EFF<sup>fl/fl</sup>Tet1/2/3<sup>fl/fl</sup>Col1a2<sup>CreER</sup>). Tamoxifen mediated induction of cre recombinase was able to significantly increase EFF expression and at the same time reduce expression of all three LoxP flanked *Tet* genes in COL1A2<sup>+</sup> expressing cells of EFF<sup>fl/fl</sup>Tet1/2/3<sup>fl/fl</sup>Col1a2<sup>CreER</sup> mice as compared to appropriate genotype controls (Fig. 4A, Fig. S9D–H). Such lowering of TET1/2/3 transcript abundance resulted in reduced global 5-hmC levels at the wound-edge of EFF<sup>fl/fl</sup>Tet1/2/3<sup>fl/fl</sup>Col1a2<sup>CreER</sup> mice indicative of deficient TET enzyme activity (Fig. S10A, B). The

beneficial effects on limb perfusion and abundance of COL1A2<sup>+</sup>VF<sub>EFF</sub><sup>+</sup> VF<sub>EFF</sub> that emerged in the ischemic tissue in EFF<sup>fl/fl</sup>Col1a2<sup>CreER</sup> mice upon tamoxifen treatment, was reduced in TET1/2/3 deficient EFF<sup>fl/fl</sup>Tet1/2/3<sup>fl/fl</sup>Col1a2<sup>CreER</sup> mice (Fig. 4B–F). Additionally, in TET1/2/3 deficient EFF<sup>fl/fl</sup>Tet1/2/3<sup>fl/fl</sup>Col1a2<sup>CreER</sup> mice, the promoter of vasculogenic genes remained hypermethylated (*Cdh5*, 87.5%; *Vwif*, 95.8%; and *Pecam1*, 87.5%) as compared to TET1/2/3 sufficient EFF<sup>fl/fl</sup>Col1a2<sup>CreER</sup> mice (*Cdh5*, 43.1%; *Vwif*, 21%; and *Pecam1*, 46.1%) upon tamoxifen treatment (Fig. 4G). These findings in transgenic mice models suggested that the presence of TET1/2/3 enzymes specifically in the COL1A2<sup>+</sup> dermal fibroblast compartment is necessary to enable the VF<sub>EFF</sub> emergence and improved perfusion of the ischemic limb skin.

### TET-dependent demethylation of fibroblast-borne endothelial genes causes the formation of vasculogenic fibroblast and rescues perfusion in diabetic ischemic limbs

Compared to non-diabetic human subjects, patients with diabetes showed lower EFF and TET1/2/3 endogenous abundance in their wound-edge tissue (Fig. S11A, B). The functional significance of low TET1/2/3 endogenous abundance was manifested as significant lowering of global 5-hmC abundance at WE in human diabetic subjects (Fig. S11C). To test this pathway in diabetic mice, leptin receptor deficient B6.BKS(D).Lepr<sup>db/db</sup> (db/db) mice were used as a type 2 diabetes model keeping non-hyperglycemic m<sup>+</sup>/db littermates as non-diabetic controls (Fig. S11D). Bisulfite sequencing of the DNA isolated from uninjured skin revealed that promoter regions of vasculogenic genes, *Cdh5* (81.5% vs 18.5%), *Vwif* (78.8% vs 21.2%) and *Pecam1* (76.4% vs 23.6%) genes remained hypermethylated in diabetic db/db as compared to non-diabetic m<sup>+</sup>/db mice (Fig. S11E). This epigenetic regulation is consistent with low expression of EFF and TET1/2/3 along with vasculogenic genes at the cutaneous WE of acutely injured db/db diabetic mice compared to m<sup>+</sup>/db controls specifically in COL1A2<sup>+</sup> dermal fibroblast rich tissue elements (Fig. S11F–I). Under this experimental setting, exogenous TNT<sub>EFF</sub> increased the abundance of TET1/2/3 at the WE in dermal fibroblasts (COL1A2<sup>+</sup>) and resulted in increased perfusion and accelerated wound closure (Fig. S11J–M). The histological presence of increased COL1A2<sup>+</sup>VF<sub>EFF</sub><sup>+</sup> VF<sub>EFF</sub> in response to EFF transfection was also reduced to basal levels when TET1/2/3 were silenced at the d14 WE (Fig. S11N). Bisulfite sequencing of the DNA isolated from dermal fibroblasts (COL1A2<sup>+</sup>) at d14 WE of db/db mice revealed that promoter regions of vasculogenic genes, *Cdh5* (35.2% methylated vs 77.4% methylated), *Vwif* (44% vs 80.5%) and *Pecam1* (39% vs 89.5%), were hypomethylated in response to EFF transfection as compared to EP controls, respectively (Fig. S11O). The observed effect of EFF delivery on vascular gene demethylation in WE tissue of db/db mice was lost when TET1/2/3 were inhibited (*Cdh5*, 84.4% methylated; *Vwif*, 88.2% methylated; *Pecam1*, 88% methylated) (Fig. S11O). To understand the effect of TNT<sub>EFF</sub> on non-diabetic m<sup>+</sup>/db controls, a





similar set of above-mentioned experiments was conducted. TNT<sub>EFF</sub> delivery in non-diabetic *m<sup>+</sup>/db* mice at the cutaneous WE of acute wounds resulted in increased perfusion and accelerated wound closure (Fig. S12A–C). The beneficial effect of *EFF* on wound perfusion and healing was delayed when *TET1/2/3* were inhibited under the same experimental conditions (Fig. S12A–C). In addition, histological presence of increased COL1A2<sup>+</sup>/VWF<sup>+</sup> V<sub>EFF</sub> in response to *EFF* transfection

was also reduced to basal levels when *TET1/2/3* were silenced at the d14 WE of non-diabetic *m<sup>+</sup>/db* wounded mice (Fig. S12D, E). In a second experimental setting of tissue ischemia in diabetic *db/db* mice, TNT<sub>EFF</sub> rescued the ischemic limb following HLI surgery, with significantly improved perfusion as measured by high resolution LSI (Fig. 5A, B) and ultrasound imaging (Fig. 5C, D). The enhanced perfusion of the diabetic ischemic limb post-*EFF* transfection was abrogated when *TET1/2/3*

**Fig. 3 | TET-dependent vasculogenic state of fibroblasts require demethylation of fibroblast-borne endothelial genes in vivo.** **A** Study design showing TNT<sub>2.0</sub> procedure and related vascular imaging in hind-limb ischemia model in C57BL/6 mice. Created in BioRender. Mohanty, S. (2024) BioRender.com/f78e778. Representative PeriMed laser speckle-assisted limb perfusion images (**B**) and quantification (**C**) of hind limb perfusion at different time points post-surgery in C57BL/6 mice treated with TNT<sub>EP+scramble</sub>, TNT<sub>EFF+scramble</sub>, TNT<sub>EFF+Tet1/2/3 shRNA</sub> or TNT<sub>scramble</sub> + Tet1/2/3 shRNA post hind-limb surgery ( $n = 7$ ). \*TNT<sub>EFF</sub> + scramble VS TNT<sub>EP+scramble</sub>; \*\*TNT<sub>EP</sub> + scramble VS TNT<sub>EP</sub> + Tet1/2/3 shRNA; \$TNT<sub>EFF</sub> + scramble VS TNT<sub>EFF</sub> + Tet1/2/3 shRNA; #TNT<sub>EFF</sub> + scramble VS TNT<sub>EP</sub> + Tet1/2/3 shRNA (one-way ANOVA, Tukey HSD post-hoc-test). One-way ANOVA, followed by Tukey HSD post-hoc-test. Representative ultrasound and flow velocity images (**D**) and quantification (**E**) of flow velocity of hind limb in C57BL/6 mice treated with combinations mentioned in (**B**). ( $n = 7$ ).

3 were silenced (Fig. 5A–D). In addition, the histological presence of increased COLIA2<sup>+</sup>/VWF<sup>+</sup> VF<sub>EFF</sub> in response to EFF transfection was also lowered to basal levels when *TET1/2/3* were silenced in ischemic hind limbs of db/db mice (Fig. 5E–G). The impact of TNT<sub>EFF</sub> was also significantly demonstrated in the increased presence of COLIA2<sup>+</sup> VF<sub>EFF</sub> comprising blood vessels that were documented to be perfused with intravenously injected lectin in the db/db mice (Fig. S13A–C). Perfused COLIA2<sup>+</sup>/VWF<sup>+</sup> VF<sub>EFF</sub> were significantly reduced when *TET1/2/3* transcripts were knocked down in the presence of TNT<sub>EFF</sub> treatment in db/db mice (Fig. S13B, C). These results demonstrate that diabetes blunts endogenous EFF and *TET1/2/3* transcript abundance in WE dermal fibroblasts upon wounding. Topical TNT<sub>EFF</sub> delivery to skin was effective in rescue.

## Discussion

In the present study, in vitro VF<sub>EFF</sub> emergence was associated with increased transcript abundance of *TET1/2/3* (Fig. 1C). A direct interaction between ETV2 and TET1/2 and FLI1 and TET2 was identified by Flag-based co-immunoprecipitation assay (Fig. 1G) and *TET1/2/3* knockdown during concomitant EFF overexpression, blunted VF<sub>EFF</sub> emergence by repressing vasculogenic genes (*VEGFR2*, *PECAMI* and *CDH5*) in EFF-treated dermal fibroblasts (Fig. S5D). A VF transcriptional scRNAseq signature was identified in EFF but not EP treated dermal fibroblasts and this signature was TET-dependent (Fig. S5B–E). TNT<sub>EFF</sub> also induced TET expression in fibroblasts in vivo and fibroblast-specific inducible overexpression of EFF induced TET expression in both sexes, led to VF transition in vivo. TET induction was associated with elevated 5-hmC abundance in VF. VF emergence required TET-dependent demethylation of fibroblast-borne endothelial genes in vivo and this effect augmented VF abundance and rescued perfusion in diabetic ischemic limbs. TNT<sub>EFF</sub> also rescued perfusion and closure of murine diabetic skin wounds and increased VF in cultured human skin explants. This work recognizes the significance of *TET1/2/3* in the TNT<sub>EFF</sub> inducible formation of VF that form de novo blood vessels to rescue diabetic ischemic tissue. Of note, in achieving functional rescue of ischemic tissue VF does not act in isolation and must rely on a broader community of cells and their microenvironmental factors at the affected site.

TET-dependent DNA demethylation at the promoter-site of developmental genes enables adaptive developmental plasticity<sup>23,24</sup>. TET-induced demethylation and elevated hydroxymethylation of promoter and enhancer sites of cell-fate determining genes enhance chromatin accessibility and drive gene expression unleashing cellular plasticity. Among genomic regions, bivalent domains characteristically possess two histone marks that are associated with both positive (“on”) and negative (“off”) transcriptional events. TET participate in the establishment and/or maintenance of bivalent domains of many differentiation-associated genes thus enabling developmental plasticity<sup>24</sup>. Tet1/2 double knockdown downregulate pluripotency-related genes such as *Esrrb* and *Prdm14*<sup>25</sup>, which are reported to safeguard embryonic cells from adopting an endoderm cell fate<sup>26</sup>,

Results represent mean  $\pm$  S.D. One-way ANOVA, followed by Tukey HSD post-hoc-test. **F** Immunofluorescence images of hind-limb ischemic skin (left) and colocalization quantification (right) of COLIA2 (green) and VWF (red) staining of 4 groups in (**B**) determined by Pearson correlation coefficient ( $r$ ). The white arrow represents the area of colocalization. Data expressed as mean  $\pm$  S.D ( $n = 7, 7, 6, 6$ ). One-way ANOVA, followed by Tukey HSD post-hoc-test. **G** Bisulfite sequencing analyses of endothelial specific gene [*Cdh5* (left), *Vwf* (middle), and *Pecam1* (right)] promoter methylation in laser capture microdissection (LCM) captured COLIA2<sup>+</sup> elements at d14 hind-limb ischemic skin of C57BL/6 mice treated with combinations mentioned in (**D**) (methylated CpG, black; unmethylated CpG, white). Number of clones = 6. Venn diagram shows the distribution of methylated and unmethylated CpGs in promoter of each gene. AU, arbitrary unit. Source data are provided as a Source Data file.

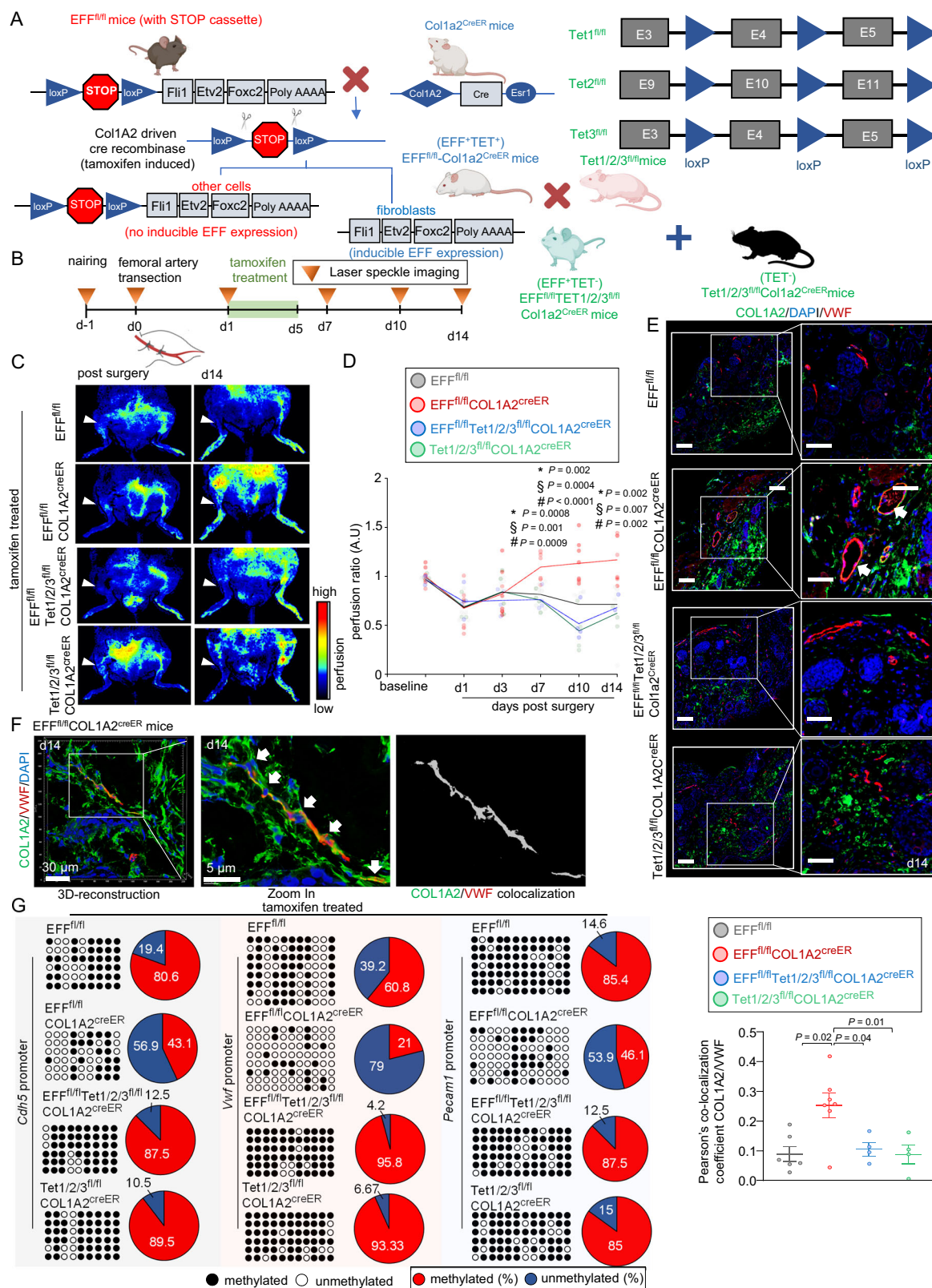
resulting in increased extra-embryonic lineage differentiation<sup>25</sup>. Thus, TET function may be viewed as a key enabler of cell plasticity.

Closed chromatin structure and related DNA methylation repress gene expression in somatic cells. Such barriers of genome plasticity hinder cell and tissue reprogramming<sup>27</sup>. Demethylation of cell-stemness enhancers occur by TF-guided recruitment of TET proteins to designated chromatin loci<sup>18,28</sup>. Because of epigenetic barriers<sup>5</sup>, success in direct reprogramming fibroblasts into different lineages has been limited<sup>6,7</sup>. ETV2 is a pioneering TF which supports the transition of cells of the primitive mesoderm to hematoendothelial lineages<sup>29</sup>. The loss of *Etv2* results in early embryonic death because of complete loss of hematoendothelial differentiation<sup>30</sup>. In endothelial development, ETV2 increases chromatin accessibility to potentiate binding of downstream TF, such as *Flil* and *Erg*, that in turn occupy promoter regions for numerous key endothelial genes<sup>5,31</sup>. In fact, sustained binding ability of *Flil* to methylation-rich regions in hematopoietic progenitor cells<sup>32</sup>, make this TF an ideal choice for fibroblast $\rightarrow$ VF<sub>EFF</sub> state change. In addition, appropriate methyltransferase-dependent Foxc2-expression is essential for early phases of lymphatic development and maturation<sup>33,34</sup>. Thus, EFF-induced vasculogenesis is subject to epigenetic regulation. Because EFF-induced vasculogenesis requires tissue hypoxia as a pre-condition, restoration of normoxia in response to induced vasculogenesis is expected to act as a stop signal serving the role of an in-built safety valve against the perils of uncontrolled vascularization.

In non-vascular cells, overexpression of ETV2 induces vascular characteristics via upregulated *TET1/2*<sup>35</sup>. Demethylation of vascular genes is a prerequisite for the conversion of somatic to vasculogenic cells<sup>7</sup>. Such processes, especially those caused by DNMT-inhibition, induce vascular characteristics<sup>36</sup> in non-vascular cells. In fibroblasts subjected to TF-induced vascular reprogramming, hypomethylation of the proximal promoters of several endothelial-specific genes is reported<sup>37</sup>. Genetic inactivation of *Tet1-3*, causing hypermethylation, in murine embryonic fibroblasts limits reprogramming efficiency<sup>37</sup>. Such epigenetic arrest of endothelial functionality is noted under conditions of hyperglycemia-induced inactivation of TET2 wherein angiogenesis is impaired<sup>38</sup>. Findings of the current study on the rescue of VF under diabetic conditions recognize a novel role of *Tet1/2/3*. In fibroblasts, high *TET1/2/3* gave rise to a specific subset (cluster 3) enriched in key vasculogenic genes and active in forming functional blood vessels. The VF<sub>EFF</sub> is an example of fibroblast heterogeneity that can be induced to form productive blood vessels achieving rescue of tissue at risk of ischemic insult. This work recognizes TET, a dioxygenase catalyst of DNA methylation, as a major contributor to the EFF-dependent induction of the VF<sub>EFF</sub>. That diabetic condition limit TET function predicts sub-optimal function of VF. TNT-based therapeutic delivery of EFF was able to bolster TET expression under conditions of diabetes and rescue blood supply to the diabetic ischemic tissue.

In conclusion, this work recognizes VF<sub>EFF</sub> as physiological and wound-inducible subset of skin fibroblasts. TET enzymes play a pivotal role in causing EFF-induced VF<sub>EFF</sub> state change. The significance of this





observation is amplified under conditions of diabetes wherein TET activity is suppressed. On its path to producing VF<sub>EFF</sub>, TNT<sub>EFF</sub> bolsters TET expression. Vasculogenic in vivo skin reprogramming involves a simple point-of-care scalable approach wherein the entire process unfolds in the body under immune surveillance obviating the need for elaborate laboratory infrastructure. TET-targeting is recognized to be productive in managing tumor outcomes<sup>39,40</sup>. This work recognizes the

significance of TET1/2/3 in the inducible formation of VF<sub>EFF</sub> to form de novo blood vessels to rescue diabetic ischemic tissue.

## Methods

Our experimental data, analytical methods, and study materials will be made available upon request to interested researchers to permit replicating the procedures and corroborating the results. A detailed

**Fig. 4 | Fibroblast-specific inducible overexpression of EFF causes induction of TET, which is followed by transition of fibroblast to vasculogenic fibroblast in vivo.** **A** pTARGATT-CAG-L4SL-Fli IRES-Etv2-T2A-Foxc2-PolyA was constructed for the generation of Foxc2, Etv2, and Fli1 knock-in (EFF<sup>f/f</sup>) mouse model. The EFF<sup>f/f</sup> mice were crossed with Col1a2<sup>CreER</sup> mice (EFF<sup>f/f</sup>Col1a2<sup>CreER</sup>) to specifically induce EFF expression in Col1a2 expressing cells upon tamoxifen application. EFF<sup>f/f</sup>Col1a2<sup>CreER</sup> mice were also crossed with Tet1/2/3<sup>f/f</sup> to generate EFF<sup>f/f</sup>Tet1/2/3<sup>f/f</sup>Col1a2<sup>CreER</sup> mice. Additional mouse colony Tet1/2/3<sup>f/f</sup>Col1a2<sup>CreER</sup> was generated. Model characterization is provided in Figs S9, 10. **B** Schematic diagram of hind-limb experiment and vascular imaging in: (i) EFF<sup>f/f</sup>, (ii) EFF<sup>f/f</sup>Col1a2<sup>CreER</sup>, (iii) EFF<sup>f/f</sup>Tet1/2/3<sup>f/f</sup>Col1a2<sup>CreER</sup> and (iv) Tet1/2/3<sup>f/f</sup>Col1a2<sup>CreER</sup>. Tamoxifen treatment was done for 5 days post-surgery. Representative PeriMed laser speckle-assisted limb perfusion images (**C**) and quantification (**D**) of hind limb perfusion at different time points in abovementioned 4 groups ( $n = 8, 8, 4, 4$ ). \*EFF<sup>f/f</sup>Col1a2<sup>CreER</sup> vs EFF<sup>f/f</sup>, #EFF<sup>f/f</sup>Col1a2<sup>CreER</sup> vs EFF<sup>f/f</sup>Tet1/2/3<sup>f/f</sup>Col1a2<sup>CreER</sup>, \*EFF<sup>f/f</sup>Col1a2<sup>CreER</sup> vs Tet1/2/3<sup>f/f</sup>Col1a2<sup>CreER</sup> (one-way ANOVA, Tukey HSD post-hoc-test). **E** Immunofluorescence

images of hind-limb ischemic skin (top) and colocalization quantification (bottom) of COL1A2 (green) and VWF (red) staining of the abovementioned groups (**B**) was determined by Pearson correlation coefficient ( $r$ ). White arrow represents colocalization. Data expressed as mean  $\pm$  S.D ( $n = 6, 7, 4, 4$ ). (one-way ANOVA, Tukey HSD post-hoc-test). **F** Immunofluorescence image of day 14 hind limb ischemic tissue in EFF<sup>f/f</sup>COL1A2<sup>CreER</sup> mice stained for COL1A2 and VWF. The left panel shows the 3D-reconstruction image of the colocalized COL1A2 and VWF rendered by IMARIS (inset). The middle panel shows the magnified inset. The right panel shows the colocalized area for COL1A2 and VWF. Scale, 30  $\mu$ m. **G** Bisulfite sequencing analyses of endothelial specific gene {*Cdh5* (left), *Vwf* (middle) and *Pecam1* (right)} promoter methylation in LCM captured COL1A2<sup>+</sup> elements for at d14 hind-limb ischemic skin of abovementioned (**B**) groups (methylated CpG, black; unmethylated CpG, white). Number of clones = 6. Venn diagram shows the distribution of methylated and unmethylated CpGs in promoter of each gene. AU, arbitrary unit. Source data are provided as a Source Data file.  $n =$  biological replicates in (**D**, **E**). **A**, **B** are created in BioRender. Mohanty, S. (2024) BioRender.com/e89c803.

“Materials and Methods” section can be found in Supplemental Material which includes primers for quantitative real-time PCR (RT-qPCR) (Supplementary Table 1) and bisulfite sequencing (Supplementary Table 2). The list of key reagents used in this study are provided in Supplementary Data 1.

### Animal care and use

All experiments and procedures conducted on animals were approved by the Indiana University School of Medicine and University of Pittsburgh Institutional Animal Care and Use Committees (IACUC).

### Murine hindlimb ischemia

Mice (8–12 weeks old) were anaesthetized using 1–3% isoflurane and unilateral femoral artery occlusion with transection and removal<sup>41</sup>. Following skin closure, buprenorphine was administered subcutaneously for pain control. Laser speckle imaging was used to confirm arterial occlusion 2 h post-operatively<sup>15,16</sup>.

### Murine cutaneous wound healing

Cutaneous wounds were created in pairs using a punch biopsy on the dorsum of the mouse equidistant from the midline and the 4 limbs. The wounds were splinted with a silicon sheet to prevent contraction as described<sup>42</sup>. Each wound was digitally photographed, and area quantitated using ImageJ software.

### In vivo collagen gel implantation

Human Adult Dermal Fibroblast cells (expressing green fluorescence protein; HADF-GFP, 1 million) treated with EFF (along with scramble), EFF (along with TET1/2/3 siRNA cocktail), and empty plasmid (along with scramble) were mixed with 1 million cord blood ECFC (expressing tdTomato) and added to 1 mL type 1 rat tail collagen solution followed by incubation at 37 °C for 48 h. The collagen gels were then picked and implanted subcutaneously beneath the ventral abdominal skin near the groin in immunodeficient mice as reported<sup>15</sup>. On day 28, mice were infused with Alexa 647-bound lectin via tail vein injection, then sacrificed, and gels were recovered for perfused vessel analysis.

### Single-cell RNA sequencing (scRNA-seq) analysis

HADF, HADF<sup>EFF+scramble</sup>, and HADF<sup>EFF+TET1/2/3 siRNA</sup> were collected at day 5 post-transfection and processed for scRNA-seq analysis per 10X Genomics protocol as reported previously<sup>15,43–45</sup>.

### Human samples

Human wound biopsy samples were obtained from clinically diagnosed diabetic and non-diabetic subjects. All human studies were

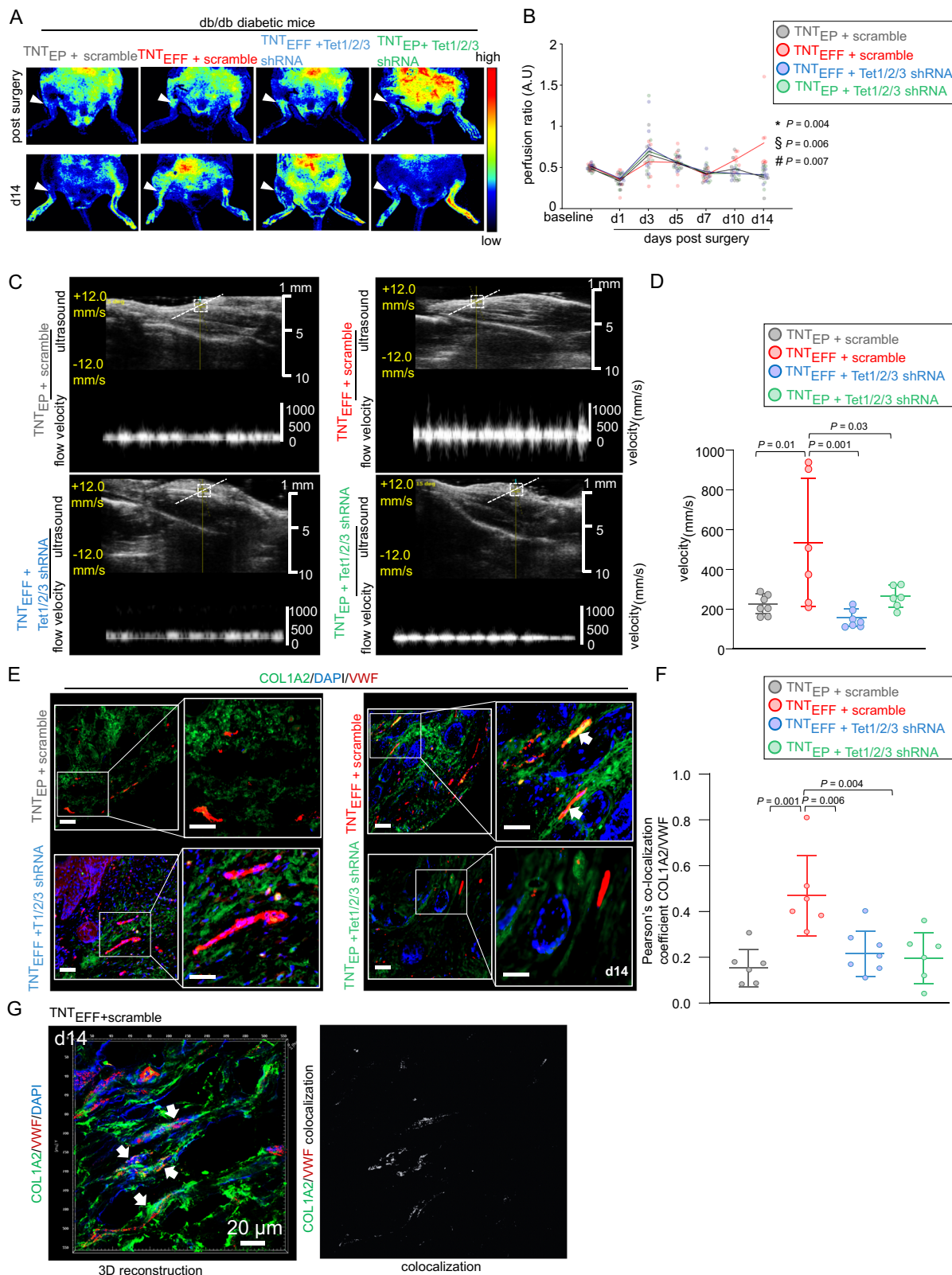
approved by the Institutional Review Board (IRB) of Indiana University (IRB#12516, Approved Protocol#1505714405) or that of University of Pittsburgh (IRB#0511186). This included the collection of wound tissue obtained from individuals undergoing wound care. In the cases of surgically discarded tissue and de-identified samples, IRB determined that informed consent was not required from the subjects per federal guidelines category #4 listed in 45CFR 46.101(b)(1) through 46.101(b)(6). The Declaration of Helsinki protocols were followed. The demographics of subjects with the location of wounds included in this study have been provided in Supplementary Table 3.

### Ex vivo cultured human skin explants

Under a protocol approved by the Institutional Review Board of the University of Pittsburgh (#0511186), surgically discarded and de-identified human skin samples were obtained from individuals undergoing surgery and processed for human skin wound ex vivo culture. The demographics of the study participants are detailed in the Supplementary Table 4. Samples were first washed with 1X PBS containing 1% antibiotic and antimycotic (cat no. p0-781, Gibco), followed by a wash with 70% ethanol, and then rinsed again with PBS. The stratum corneum was removed using a Zimmer Electric Dermotome, and ~500–600  $\mu$ m of tissue was collected. The collected tissue was trimmed into 1  $\times$  1 cm rectangular shapes and placed in 6 well culture plates containing RPMI 1640 High Glucose medium containing 25 mM of D-glucose (cat no. 11875119, Gibco) supplemented with 10% Fetal bovine serum and 1% antibiotic. At day 1 post-wounding, TNT<sub>EP</sub> ( $n = 9$  grafts from 5 individuals) or TNT<sub>EFF</sub> ( $n = 10$  grafts from the same 5 individuals) was performed on epidermal side of grafts and cultured for a total of 7 days with daily media changes. Digital images were also captured on day 3 and day 7 to observe the physical condition of the tissue grafts. After 7 days, the wound tissues were fixed in 4% paraformaldehyde (PFA) or processed for paraffin tissue sections, antigen retrieval, immunofluorescent staining, and imaging.

### CO-Detection by indEXing (CODEX) method using PhenoCycler-Fusion

Tissue antigen retrieval was conducted as per instructions by the Akoya Biosciences protocol. After antigen retrieval and tissue hydration, fixation for staining was carried out. An antibody cocktail was formulated with the specified antibodies and applied to the tissues. Subsequently, another fixation step was performed to ensure adherence of the tissue to the slide in preparation for washing cycles during imaging. The staining employed the antibody CD31 (cat no. 92841SF, CST) (1:200 dilution), barcodes, and their respective reporters as -BX002 (custom conjugated (5450023)–Atto 550-RX002. Imaging was



conducted at 20X resolution using the fully automated CODEX system (Akoya Biosciences) and a Phenolmager slide scanning microscope. Sample processing, analysis, and visualization were performed using Phenochart software 2.0, and the microvessel density was calculated using Vessel Analysis plugin and the Mexican Hat filter plugin for FIJI/ImageJ (NIH).

### Statistical analyses

Statistical analyses was performed using GraphPad Prism version 10 (GraphPad Software). Data throughout the article are expressed as mean  $\pm$  SD. The results were analyzed by Student's *t* test (two-tailed) to determine significant differences. Comparison between multiple groups were tested using analysis of variance (ANOVA). Tukey's



**Fig. 5 | TET-dependent demethylation of fibroblast-borne endothelial genes in dermal fibroblast causes the formation of vasculogenic fibroblast and rescues perfusion in diabetic ischemic limbs.** Representative PeriMed laser speckle-assisted limb perfusion images at d14 (A) and its quantification (B) of hind limb perfusion at different time points post-surgery in db/db mice treated with  $\text{TNT}_{\text{EP+scramble}}$ ,  $\text{TNT}_{\text{EFF+scramble}}$ ,  $\text{TNT}_{\text{EFF+Tet1/2/3 shRNA}}$  and  $\text{TNT}_{\text{EP+Tet1/2/3 shRNA}}$  post hind-limb surgery ( $n = 7$ ). \* $\text{TNT}_{\text{EFF+scramble}}$  vs  $\text{TNT}_{\text{EP+scramble}}$ ;  $\text{TNT}_{\text{EFF+scramble}}$  vs  $\text{TNT}_{\text{EFF+Tet1/2/3 shRNA}}$ ; # $\text{TNT}_{\text{EFF+scramble}}$  vs  $\text{TNT}_{\text{EP+Tet1/2/3 shRNA}}$  (one-way ANOVA, Tukey HSD post-hoc-test). The study design and time points are similar to Fig. 3A. C Representative ultrasound and flow velocity images and quantification (D) of the flow velocity of the hind limb in db/db mice treated with combinations mentioned in (B)

( $n = 7, 6, 7, 6$ ). One-way ANOVA, Tukey HSD post-hoc-test. Results represent mean  $\pm$  S.D. E Immunofluorescence images of hind-limb ischemic skin and colocalization quantification (F) of COL1A2 (green) and VWF (red) staining of the abovementioned groups (B) were determined by Pearson correlation coefficient ( $r$ ). The white arrow represents the area of colocalization. Data expressed as mean  $\pm$  S.D. ( $n = 6, 6, 7, 6$ ). One-way ANOVA, Tukey HSD post-hoc-test). AU, arbitrary unit. G Immunofluorescence confocal image of day 14 hind limb ischemic tissue in  $\text{TNT}_{\text{EFF+scramble}}$  db/db mice stained for COL1A2 and VWF. The left panel shows the 3D-reconstruction image of the colocalized COL1A2 and VWF rendered by IMARIS software (inset). The middle panel shows the magnified inset. The right panel shows the colocalized area for COL1A2 and VWF. Scale, 20  $\mu\text{m}$ . Source data are provided as a Source Data file.

honestly significant difference (HSD) post hoc test was applied.  $P < 0.05$  was considered statistically significant.

### Reporting summary

Further information on research design is available in the Nature Portfolio Reporting Summary linked to this article.

### Data availability

Source data are provided with this paper. The raw single cell RNA sequencing data generated in this study have been deposited in the GEO database under accession number GSE167406. Bisulfite sequencing data have been deposited in BioProject with accession number PRJNA1175408. Source data are provided in the Source Data file. Source data are provided with this paper.

### Code availability

No Original codes were written for this manuscript. Scripts for the downstream analysis of the single-cell data are available on GitHub [https://github.com/RajneeshSrivastava/EFF\\_Analysis](https://github.com/RajneeshSrivastava/EFF_Analysis). Citable code is available at: <https://doi.org/10.5281/zenodo.13942154>.

### References

1. Srivastava, D. & DeWitt, N. In vivo cellular reprogramming: the next generation. *Cell* **166**, 1386–1396 (2016).
2. Larouche, J. & Aguilar, C. A. New technologies to enhance in vivo reprogramming for regenerative medicine. *Trends Biotechnol.* **37**, 604–617 (2019).
3. Kelaini, S., Cochrane, A. & Margariti, A. Direct reprogramming of adult cells: avoiding the pluripotent state. *Stem Cells Cloning* **7**, 19–29 (2014).
4. Graf, T. & Enver, T. Forcing cells to change lineages. *Nature* **462**, 587–594 (2009).
5. Wingo, M. & Rafii, S. Endothelial reprogramming for vascular regeneration: past milestones and future directions. *Semin. Cell Dev. Biol.* **122**, 50–55 (2022).
6. Han, J. K. et al. Direct conversion of adult human fibroblasts into functional endothelial cells using defined factors. *Biomaterials* **272**, 120781 (2021).
7. Han, J. K. et al. Direct conversion of adult skin fibroblasts to endothelial cells by defined factors. *Circulation* **130**, 1168–1178 (2014).
8. Morita, R. et al. ETS transcription factor ETV2 directly converts human fibroblasts into functional endothelial cells. *Proc. Natl Acad. Sci. USA* **112**, 160–165 (2015).
9. Chen, T. et al. DKK3 (Dkkopf-3) transdifferentiates fibroblasts into functional endothelial cells—brief report. *Arterioscler. Thromb. Vasc. Biol.* **39**, 765–773 (2019).
10. Liu, Z. et al. Re-patterning of H3K27me3, H3K4me3 and DNA methylation during fibroblast conversion into induced cardiomyocytes. *Stem Cell Res.* **16**, 507–518 (2016).
11. Oh, S. Y., Kim, J. Y. & Park, C. The ETS factor, ETV2: a master regulator for vascular endothelial cell development. *Mol. Cells* **38**, 1029–1036 (2015).
12. Park, S. Y. et al. ETV2- and Flt1-induced vascular progenitor cells enhance functional recovery in ischemic vascular disease model—brief report. *Arterioscler. Thromb. Vasc. Biol.* **40**, e105–e113 (2020).
13. Lee, S. et al. Direct reprogramming of human dermal fibroblasts into endothelial cells using ER71/ETV2. *Circ. Res.* **120**, 848–861 (2017).
14. Wong, W. T., Huang, N. F., Botham, C. M., Sayed, N. & Cooke, J. P. Endothelial cells derived from nuclear reprogramming. *Circ. Res.* **111**, 1363–1375 (2012).
15. Pal, D. et al. Identification of a physiologic vasculogenic fibroblast state to achieve tissue repair. *Nat. Commun.* **14**, 1129 (2023).
16. Gallego-Perez, D. et al. Topical tissue nano-transfection mediates non-viral stroma reprogramming and rescue. *Nat. Nanotechnol.* **12**, 974–979 (2017).
17. Lemmerman, L. R. et al. Nanotransfection-based vasculogenic cell reprogramming drives functional recovery in a mouse model of ischemic stroke. *Sci. Adv.* **7**, eabd4735 (2021).
18. Sardina, J. L. et al. Transcription factors drive Tet2-mediated enhancer demethylation to reprogram cell fate. *Cell Stem Cell* **23**, 727–741.e729 (2018).
19. Wu, X. & Zhang, Y. TET-mediated active DNA demethylation: mechanism, function and beyond. *Nat. Rev. Genet.* **18**, 517–534 (2017).
20. Tanaka, T. et al. ETV2-TET1/TET2 complexes induce endothelial cell-specific robo4 expression via promoter demethylation. *Sci. Rep.* **8**, 5653 (2018).
21. Dunn, J. et al. Flow-dependent epigenetic DNA methylation regulates endothelial gene expression and atherosclerosis. *J. Clin. Invest.* **124**, 3187–3199 (2014).
22. Pirola, L. et al. Genome-wide analysis distinguishes hyperglycemia regulated epigenetic signatures of primary vascular cells. *Genome Res* **21**, 1601–1615 (2011).
23. Dawlaty, M. M. et al. Combined deficiency of Tet1 and Tet2 causes epigenetic abnormalities but is compatible with postnatal development. *Dev. Cell* **24**, 310–323 (2013).
24. Wu, X., Li, G. & Xie, R. Decoding the role of TET family dioxygenases in lineage specification. *Epigenetics Chromatin* **11**, 58 (2018).
25. Ficiz, G. et al. Dynamic regulation of 5-hydroxymethylcytosine in mouse ES cells and during differentiation. *Nature* **473**, 398–402 (2011).
26. Ma, Z., Swigut, T., Valouev, A., Rada-Iglesias, A. & Wysocka, J. Sequence-specific regulator Prdm14 safeguards mouse ESCs from entering extraembryonic endoderm fates. *Nat. Struct. Mol. Biol.* **18**, 120–127 (2011).
27. Fu, X. et al. Restricting epigenetic activity promotes the reprogramming of transformed cells to pluripotency in a line-specific manner. *Cell Death Discov.* **9**, 245 (2023).

28. Schwarz, B. A. et al. Prospective isolation of poised iPSC intermediates reveals principles of cellular reprogramming. *Cell Stem Cell* **23**, 289–305.e285 (2018).
  29. Koyano-Nakagawa, N. & Garry, D. J. ETV2 as an essential regulator of mesodermal lineage development. *Cardiovasc Res* **113**, 1294–1306 (2017).
  30. Lee, D. et al. ER1 acts downstream of BMP, Notch, and Wnt signaling in blood and vessel progenitor specification. *Cell Stem Cell* **2**, 497–507 (2008).
  31. Abedin, M. J. et al. Flt1 acts downstream of ETV2 to govern cell survival and vascular homeostasis via positive autoregulation. *Circ. Res.* **114**, 1690–1699 (2014).
  32. Hogart, A. et al. Genome-wide DNA methylation profiles in hematopoietic stem and progenitor cells reveal overrepresentation of ETS transcription factor binding sites. *Genome Res.* **22**, 1407–1418 (2012).
  33. Yoo, H. et al. Epigenetic priming by Dot1l in lymphatic endothelial progenitors ensures normal lymphatic development and function. *Cell Death Dis.* **11**, 14 (2020).
  34. Norrmen, C. et al. FOXC2 controls formation and maturation of lymphatic collecting vessels through cooperation with NFATc1. *J. Cell Biol.* **185**, 439–457 (2009).
  35. Zhang, X., Zhang, Y., Wang, C. & Wang, X. TET (Ten-eleven translocation) family proteins: structure, biological functions and applications. *Signal Transduct. Target Ther.* **8**, 297 (2023).
  36. Banerjee, S. & Bacanamwo, M. DNA methyltransferase inhibition induces mouse embryonic stem cell differentiation into endothelial cells. *Exp. Cell Res.* **316**, 172–180 (2010).
  37. Caldwell, B. A. et al. Functionally distinct roles for TET-oxidized 5-methylcytosine bases in somatic reprogramming to pluripotency. *Mol. Cell* **81**, 859–869.e858 (2021).
  38. Shi, Y. et al. Loss of TET2 impairs endothelial angiogenesis via downregulating STAT3 target genes. *Cell Biosci.* **13**, 12 (2023).
  39. Bensberg, M., et al. TET2 as a tumor suppressor and therapeutic target in T-cell acute lymphoblastic leukemia. *Proc. Natl. Acad. Sci. USA* **118**, e2110758118 (2021).
  40. Kim, H., Jung, I., Lee, C. H., An, J. & Ko, M. Development of novel epigenetic anti-cancer therapy targeting TET proteins. *Int J. Mol. Sci.* **24**, 16375 (2023).
  41. Rustagi, Y. et al. Endothelial phospholipase Cgamma2 improves outcomes of diabetic ischemic limb rescue following VEGF therapy. *Diabetes* **71**, 1149–1165 (2022).
  42. Singh, K. et al. Cutaneous epithelial to mesenchymal transition activator ZEB1 regulates wound angiogenesis and closure in a glyemic status-dependent manner. *Diabetes* **68**, 2175–2190 (2019).
  43. Singh, K. et al. Genome-wide DNA hypermethylation opposes healing in patients with chronic wounds by impairing epithelial-mesenchymal transition. *J. Clin. Investig.* **132**, e157279 (2022).
  44. Srivastava, R. et al. Human fetal dermal fibroblast-myeloid cell diversity is characterized by dominance of pro-healing Annexin1-FPR1 signaling. *iScience* **26**, 107533 (2023).
  45. Gordillo, G. M. et al. Tissue nanotransfection causes tumor regression by its effect on nanovesicle cargo that alters microenvironmental macrophage state. *Mol. Ther.* **31**, 1402–1417 (2023).
- W81XWH-21-1-0033 to C.K.S. and W81XWH-22-1-0146, HT94252410131 to K.S. Research programs led by C.K.S. were supported by the John Templeton foundation grant ID-61742 and Lilly Endowment INCITE (Indiana Collaborative Initiative for Talent Enrichment) program. We thank Professor Yong-hui Jiang (Yale University, New Haven, CT) for providing Tet1<sup>fllox/flox</sup> mice. We thank Dr. Michael Murphy for his contribution in the validation of results in clinical specimens. We also thank Julie McCormack and Diamond Reese for their technical help in performing the experiments.

## Author contributions

Conceptualization: C.K.S. Methodology: S.K.M., K.S., R.S., S.Kh.; Software: R.S. Investigation: M.K., S.Kh., S.S.V., S.C.G., S.K., S.G., R.P., Y.R., P.V., A.K.S., M.E., P.B., C.K.S.; Validation: S.K.M., K.S., M.K.; Formal Analysis: S.K.M., K.S., R.S.; Resources: S.Kh., S.R., J.P.R., M.C.Y., C.K.S.; Data Curation: R.S.; Writing—Original Draft: M.C.Y., C.K.S., S.K.M., K.S.; Writing—Review: M.C.Y., C.K.S., J.P.R., S.K.M., K.S.; Visualization: S.K.M., K.S., R.S.; Supervision: S.R., M.C.Y., J.P.R., C.K.S.; Project Administration: S.K.M., K.S., C.K.S.; Funding Acquisition: C.K.S., S.R. and K.S.

## Competing interests

The authors declare no competing interests.

## Additional information

**Supplementary information** The online version contains supplementary material available at <https://doi.org/10.1038/s41467-024-54385-w>.

**Correspondence** and requests for materials should be addressed to Chandan K. Sen.

**Peer review information** *Nature Communications* thanks the anonymous reviewers for their contribution to the peer review of this work. A peer review file is available.

**Reprints and permissions information** is available at <http://www.nature.com/reprints>

**Publisher's note** Springer Nature remains neutral with regard to jurisdictional claims in published maps and institutional affiliations.

**Open Access** This article is licensed under a Creative Commons Attribution-NonCommercial-NoDerivatives 4.0 International License, which permits any non-commercial use, sharing, distribution and reproduction in any medium or format, as long as you give appropriate credit to the original author(s) and the source, provide a link to the Creative Commons licence, and indicate if you modified the licensed material. You do not have permission under this licence to share adapted material derived from this article or parts of it. The images or other third party material in this article are included in the article's Creative Commons licence, unless indicated otherwise in a credit line to the material. If material is not included in the article's Creative Commons licence and your intended use is not permitted by statutory regulation or exceeds the permitted use, you will need to obtain permission directly from the copyright holder. To view a copy of this licence, visit <http://creativecommons.org/licenses/by-nc-nd/4.0/>.

© The Author(s) 2024

## Acknowledgements

This work was supported in part by the National Institute of Diabetes and Digestive and Kidney Diseases (NIDDK) grants DK141513, DK128845, DK135447, DK125835 and DK119099 to C.K.S. and DK136814 to K.S. This work was also supported in part by U.S. Department of Defense grants